Large Eddy Simulation of Cryogenic Injection Processes at Supercritical Pressure*

Joseph C. Oefelein
Combustion Research Facility
Sandia National Laboratories, Livermore, CA 94551-0960

Abstract

This paper highlights results from the first of a series of hierarchical simulations aimed at assessing the modeling requirements for application of the large eddy simulation technique to cryogenic injection and combustion processes in liquid rocket engines. The focus is on liquid-oxygen–hydrogen coaxial injectors at a condition where the liquid-oxygen is injected at a subcritical temperature into a supercritical environment. For this situation a diffusion dominated mode of combustion occurs in the presence of exceedingly large thermophysical property gradients. Though continuous, these gradients approach the behavior of a contact discontinuity. Significant real gas effects and transport anomalies coexist locally in colder regions of the flow, with ideal gas and transport characteristics occurring within the flame zone. The current focal point is on the interfacial region between the liquid-oxygen core and the coaxial hydrogen jet where the flame anchors itself.

INTRODUCTION

Simulating injection, mixing and combustion processes in cryogenic rocket engines poses a variety of challenges, which include all of the classical closure problems inherent to the treatment of combustion, and a unique set of problems imposed by the introduction of thermodynamic nonidealities and transport anomalies. Flow conditions within the chamber are inherently turbulent and highly transient. Significant real gas effects are present, along with the complicating factors of chemical kinetics, highly nonlinear source terms, and a variety of subgrid-scale (*sgs*) velocity and scalar mixing processes. The situation is compounded at elevated pressures due to the inherent decrease in turbulence scales and difficulties that arise as fluid states exceed local critical conditions. In this paper select results from the first of a series of hierarchical simulations are presented that focus on liquid-oxygen–hydrogen ($LOX–H_2$) coaxial injection and combustion processes. Emphasis has been placed on transcritical phenomena, where LOX is injected at a subcritical temperature into a supercritical environment. For this situation a diffusion dominated mode of combustion occurs in the presence of exceedingly large thermophysical property gradients. The focal point is on the near-field thermophysical state and flow characteristics in the vicinity of the $LOX–H_2$ interface. These initial simulations were performed as a precursor to a full production LES to better understand the nature of the interface and the associated *(sgs)* modeling requirements. The paper is organized in three parts. First the key phenomenological trends and flow characteristics are presented with a summary of the implications related to modeling. An outline of the theoretical-numerical approach is presented. Then a representative set of results are presented that highlight some of the key phenomenological trends that must be considered. Conclusions are drawn accordingly.

PHENOMENOLOGICAL TRENDS

Shear coaxial injection processes in liquid rocket engines exhibit two distinct modes of combustion. At subcritical chamber pressures, injected liquid jets undergo the classical cascade of processes associated with atomization. Dynamic forces and surface tension promote the formation of a heterogeneous spray that evolves continuously. Spray

*Approved for public release, distribution unlimited. This work performed under contract H-33477D with NASA Marshall Space Flight Center.

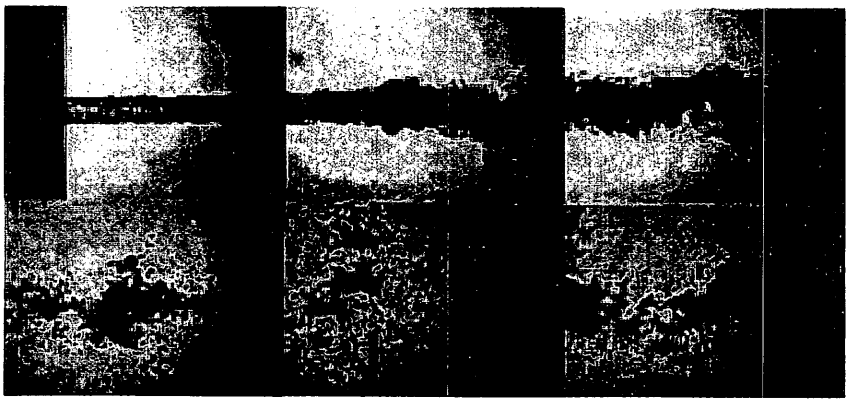

Figure 1: Reacting shear-coaxial liquid-oxygen–hydrogen injector operating at 1.5 *MPa* (15 atm). From Mayer and Tamura[1]. Used with permission.

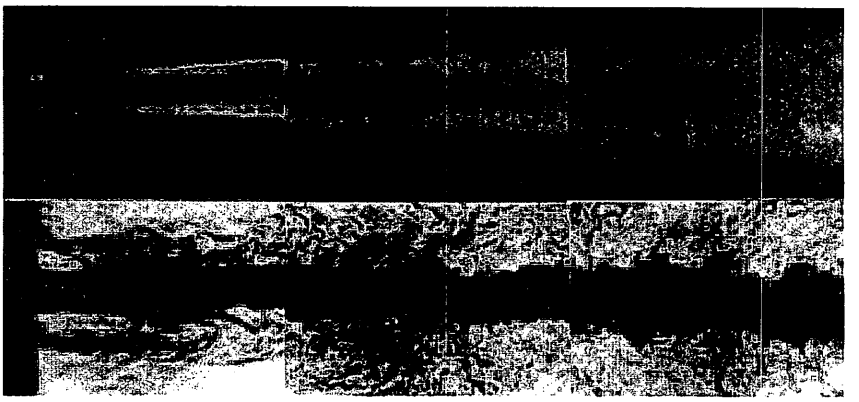

Figure 2: Reacting shear-coaxial liquid-oxygen–hydrogen injector operating at 4.5 *MPa* (44 atm). From Mayer and Tamura[1]. Used with permission.

flames form as a consequence that are lifted away from the injector face in a manner consistent with the combustion mechanisms exhibited by local drop clusters. When chamber pressures approach or exceed the critical pressure of a particular propellant, however, injected liquid jets undergo a transcritical change of state as interfacial fluid temperatures rise above the critical temperature of the local mixture. For this situation, diminished intermolecular forces promote diffusion dominated processes prior to atomization and respective jets vaporize in the presence of exceedingly large thermophysical gradients. Well mixed diffusion flames evolve as a consequence that are anchored by small but intensive recirculation zones that exist in the shearlayers between adjacent propellant streams.

The flow visualization studies conducted by Mayer and Tamura[1] have illustrated these trends for the case of a LOX–H_2 shear-coaxial injector element. The two extremes are shown in Figs. 1 and 2, respectively. Note that the critical pressure and temperature of oxygen are p_c = 5.04 *MPa* (49.7 atm) and T_c = 155 *K*, respectively. The critical pressure and temperature of hydrogen are p_c = 1.30 *MPa* (12.8 atm), T_c = 33.2 *K*. When LOX is injected at low-subcritical pressures (Fig. 1) atomization occurs forming a distinct spray as described above. Ligaments are detached from the jet surface forming spherical drops that subsequently breakup and vaporize. As the chamber pressure approaches the thermodynamic critical pressure of the LOX (Fig. 2), the number of drops present diminishes. Here, the injected LOX jet exhibits a pure diffusion mechanism at a pressure of 4.5 *MPa*, which is slightly below the thermodynamic critical pressure of oxygen, and significantly above that of hydrogen. Experimental results have revealed that flame attachment occurs instantaneously after ignition in the small but intensive recirculation zone that forms just downstream of the annular post.

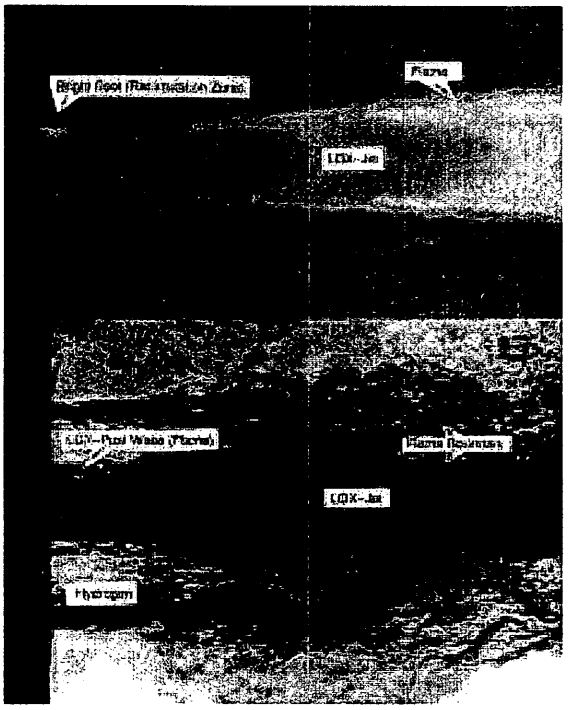

Figure 3: Near injector region of a reacting liquid-oxygen–gaseous-hydrogen shear-coaxial injector, flame (top) and corresponding flow field (bottom). Oxygen and hydrogen velocities are 30 and 300 m/s, respectively, oxygen and hydrogen injection temperatures are 100 K and 300 K, oxygen jet diameter is 1 mm, chamber pressure is 4.5 MPa (44 atm). From Mayer and Tamura [1]. Used with permission.

Simulating either of the two extremes described above requires a detailed representation of the broadband turbulence coupled with an appropriate set of thermochemical, thermodynamic and transport models. Here the focus is on the processes depicted in Fig. 2. The broadband turbulence characteristics that must be considered for this case are clearly evident Fig. 3. This figure highlights the near injector region in the vicinity of the LOX post. The mean flame characteristics are shown on the top of the figure, and the corresponding flow field is shown on the bottom. Key quantitative details are listed in the caption. The corresponding thermophysical behavior for oxygen is shown in Fig. 4. Plots of density, specific heat, viscosity, and thermal conductivity are given on the interval $40 \leq T \leq 1000\ K$ for pressures of 1, 10, 50, 100, 200, and 400 atmospheres. Note that at 1000 K and above, both oxygen and hydrogen exhibit ideal gas behavior and the pressure effect is negligible. As the temperature is decreased below 1000 K, however, nonidealities are introduced, with the property variations associated with oxygen producing the most significant effects.

Qualitative analysis of Fig. 3, when correlated with the trends shown in Fig. 4 (and similar plots of the transport properties) indicates that there are at least seven fundamentally important flow characteristics that must be accounted for simultaneously: 1) transient broadband turbulent mixing over a wide range of scales, 2) dense near-critical and supercritical fluid mixture properties, 3) strong multicomponent behavior and property gradients, 4) dominant preferential diffusion processes, 5) anomalous multiphase interfaces, 6) high pressure chemical kinetics, and 7) geometrically dominated, wall-bounded, three-dimensional evolution. Treating this set of characteristics represents a minimal requirement for any simulation-based or modeled treatment of the flow. The baseline trade-offs, algorithmic requirements, and validation requirements related to the widely used Reynolds-Averaged Navier-Stokes (RANS) approximation, Large Eddy Simulation (LES), and Direct Numerical Simulation (DNS) techniques have recently been summarized in the Proceedings of the Second International Workshop on Rocket Combustion Modeling [3].

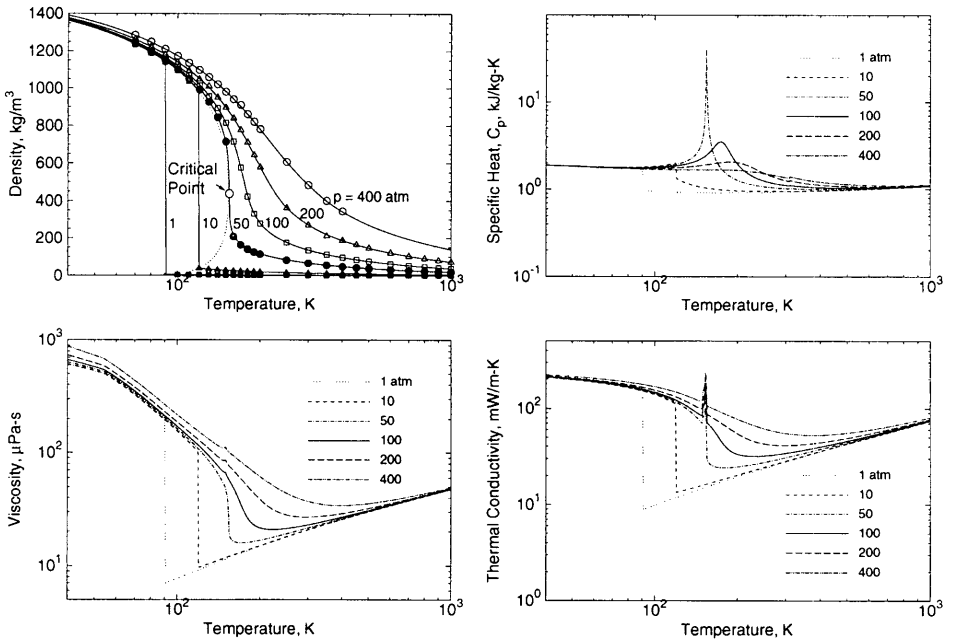

Figure 4: Density (compared with experimental data points obtained by Vargaftik [2]), specific heat, viscosity, and thermal conductivity versus temperature over the interval $40 \leq T \leq 1000$ and pressures of 1, 10, 50, 100, 200, and 400 atmospheres for pure oxygen.

THEORETICAL–NUMERICAL FRAMEWORK

The results shown here were obtained using a numerical framework developed by Oefelein [4]. This framework is appropriate for both DNS and LES and solves the fully coupled conservation equations of mass, momentum, total-energy and species. The baseline formulation handles a generalized treatment of the equation of state, thermodynamics, transport processes, and chemical kinetics for the full multicomponent system. Both ordinary and cross-diffusion terms (Dufour and Soret effects) are considered. The numerical formulation treats the fully compressible conservation equations, but can be evaluated in the incompressible limit. Thus, incompressiblity is treated as a limiting extreme of the more general compressible equation set. A unique dual-time multistage scheme is employed with a generalized preconditioning methodology that optimally treats convective, diffusive, geometric, and source term anomalies in a unified manner. This scheme employs a staggered methodology in generalized curvilinear coordinates. The algorithm has been optimized to provide excellent parallel scalability attributes using a multiblock domain decomposition with distributed-memory message-passing.

To account for thermodynamic nonidealities and transport anomalies over a wide range of pressures and temperatures, an extended corresponding states model [5,6] is employed with a cubic equation of state. In past studies [7,8] modified versions of both the Benedict-Webb-Rubin *(BWR)* equation of state and cubic equations of state have been used to evaluate the p-v-T behavior of the inherent dense multicomponent mixtures. Use of modified *BWR* equations of state in conjunction with the extended corresponding states principle has been shown to provide consistently accurate results over the widest range of pressures, temperatures and mixture states, especially at near-critical conditions. A major disadvantage of *BWR* equations, however, is that they are not computationally efficient.

Cubic equations of state can be less accurate, especially for mixtures at near-critical or saturated conditions, but are computationally efficient. Experience has shown that that both the Soave-Redlich-Kwong *(SRK)* and Peng-Robinson *(PR)* equations, when used in conjunction with the corresponding states principle, can give accurate results over the range of pressures, temperatures and mixture states of interest in this study. The *SRK* coefficients are fit to vapor

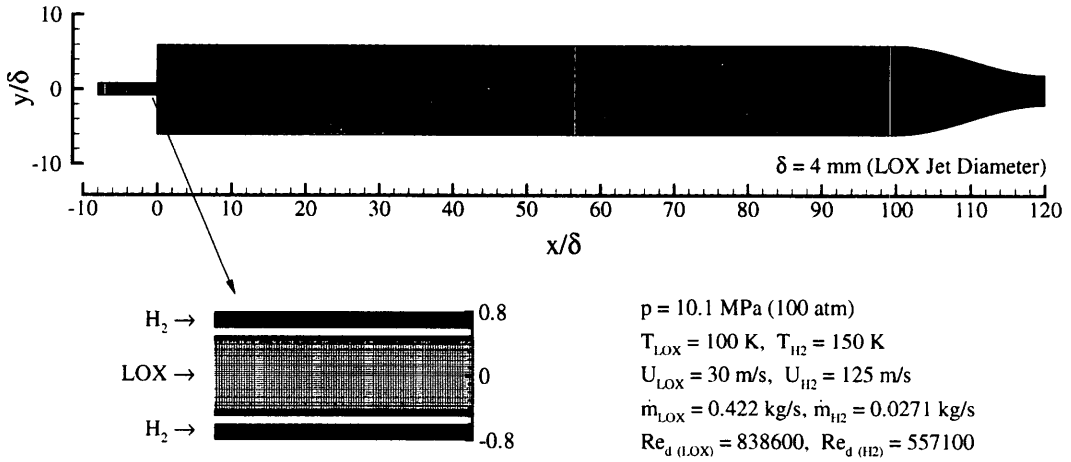

Figure 5: Schematic diagram of computational domain and flow conditions.

pressure data and are thus more suitable for conditions when the reduced temperature is less than one. The *PR* coefficients, on the other hand, are more suitable for conditions when the reduced temperature is greater than one. Because the flow involves heat release, the *PR* equation of state was used exclusively here. A summary of the cubic equations of state and recommended constants is given by Reid et al. [9], Chapter 3.

Having established an analytical representation for real mixture *p-v-T* behavior, the thermodynamic properties are obtained in two steps. First, respective component properties are combined at a fixed temperature using the extended corresponding states methodology outlined above to obtain the mixture state at a given reference pressure. A pressure correction is then applied using departure functions of the form given by Reid et al. [9], Chapter 5. These functions are exact relations derived using the Maxwell relations (see VanWylen and Sonntag [10], Chapter 10, for example) and make full use of the real mixture *p-v-T* path dependencies dictated by the equation of state. Standard state properties are obtained using the databases develop by Gordon and McBride [11] and Kee et al. [12]. Chemical potentials and fugacity coefficients are obtained in a manner similar to that outlined above.

Molecular transport properties are evaluated in a manner analogous to the thermodynamic properties. Viscosity and thermal conductivity are obtained using the extended corresponding states methodologies developed by Ely and Hanley [13,14]. The mass diffusion coefficients and thermal diffusion coefficients are obtained using the methodologies outlined by Bird et al. [15] and Hirschfelder et al. [16] in conjunction with the corresponding states methodology proposed by Takahashi [17]. Finite-rate hydrogen-oxygen kinetics are employed using the 9 species (H_2, O_2, OH, H_2O, H, O, HO_2, H_2O_2, N_2), 19-step mechanism developed by Westbrook and Dryer [18] and optimized by Yetter et al. [19].

ANALYSIS OF LOX–H_2 COAXIAL INJECTION PROCESSES

In this paper select results from the first of a series of hierarchical simulations are presented that focus on LOX–H_2 coaxial injection processes analogous to those shown in Figs. 2 and 3. The focal point is on the near-field thermo-physical state and flow characteristics of the interfacial region that separates the LOX core and the coaxial hydrogen jet. Though continuous, large gradients exist in this region that approach the behavior of a contact discontinuity. This has significant numerical implications, especially for LES. These initial simulations were performed as a precursor to a full production LES to better understand the nature of the interface and the associated modeling requirements.

The computational domain is shown in Fig. 5. This geometry generically matches the DLR windowed combustor (BK C) that is operated at high-pressure in test facility P8 [20]. The baseline configuration is cylindrical, with a uniele-

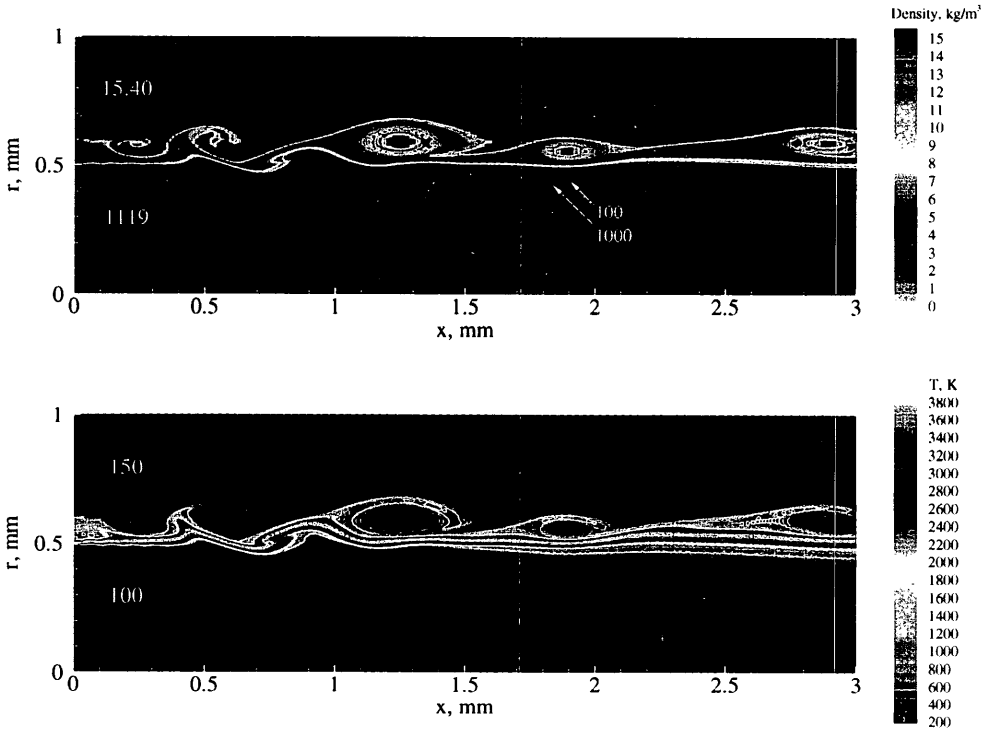

Figure 6: Contours of density and temperature in the region from the injector tip to 3 diameters downstream. Chamber pressure is 10.1 *MPa* (100 atm), hydrogen (upper stream) and oxygen (lower stream) velocities are 125 and 30 m/s, respectively, and injection temperatures are 150 *K* and 100 *K*.

ment LOX–H_2 shear-coaxial injector mounted on the centerline of the face plate and a converging nozzle at the exit. The computational domain has been nondimensionalized using a reference length scale of $\delta = 4\ mm$, which is the physical diameter of the LOX jet. The dimensionless inner and outer diameters of the annular H_2 jet are 1.2 and 1.8, respectively. The chamber and nozzle assembly is 120 dimensionless units long and the chamber diameter is 12 units.

Currently, all wall surfaces are assumed to be hydraulically smooth and adiabatic. The flow inside the injector ducts is turbulent and the velocity profiles are assumed to be fully developed. Respective mass flow rates are held constant at the inlets and time-dependent velocity profiles are specified by recycling profiles from planes at an axial distance of -2 dimensionless units back to the injector inlet, which is an axial distance of -8 dimensionless units upstream of the face plate. A constant pressure condition was applied at the nozzle exit. The simulation was performed using the mean pressure and injection conditions specified in Fig. 5. Because they are preliminary, these precursory calculations were performed on a 30 degree cylindrical sector with periodic conditions specified in the azimuthal direction. A 1.6 million cell multiblock grid was employed.

Figure 6 shows contours of density and temperature in the region from the injector tip to 3 diameters downstream. The chamber pressure is 10.1 *MPa* (100 atm). The hydrogen (upper stream) and oxygen (lower stream) velocities are 125 and 30 m/s, respectively, and the injection temperatures are 150 *K* and 100 *K*. These conditions produce a supercritical hydrogen stream and a LOX stream that undergoes a transcritical change of state in the combustion chamber. The corresponding densities are 15.4 kg/m^3 and 1119 kg/m^3, respectively. Because of the liquid-like characteristics of the oxygen, an extremely large density gradient exists. Note that the change in density is on the order of 1000 to 1. This change occurs in the near-field region of the injector over an interval that is a fraction of the LOX post thickness. In the current geometry this thickness is 0.1 dimensionless units (0.4 *mm*). Combustion occurs at near stoichiometric conditions and produces a wake that effectively separates the hydrogen and oxygen streams as the flow evolves downstream. The density is lowest in the hot reaction zone and the flame is attached to the LOX post

tip. The experimental studies of Mayer et al. [1,21] have demonstrated that in the absence of a perturbing force this flame attachment mechanism is always present.

The corresponding contours of H_2, O_2, H_2O and OH mass fractions are shown in Fig. 7. Mixing of hydrogen with hot products occurs just downstream of the LOX post. In contrast, the oxygen stream evolves relatively unimpeded compared to the product mixture in the shearlayer. The remarkable smoothness of the LOX jet is in part due to the rapid heating and vaporization of the oxygen surface. Diminished mass diffusion rates are also evident in that the oxygen is completely consumed within the flame zone. The presence of low density fluid within the shearlayer induces a vortical structure which is analogous to that produced by a backward facing step. This structure emanates from the boundary layer upstream in the annular hydrogen jet and is amplified downstream by coalescence with adjacent vortices. The combined effect produces a fuel rich flame that anchors itself to the oxygen jet and behaves in a qualitatively similar manner as the diffusion dominated flame depicted in Figs. 2 and 3.

Figure 8 shows a series of steamtraces superimposed on contours of hydrogen mass fraction in the vicinity of the LOX post. The legend corresponds to that given for H_2 in Fig. 7. The white contours highlight the location of the OH radicals, which is indicative of the flame location. Analysis of the flow structure indicates that the flame holding mechanism can be attributed to the back flow of hydrogen rich preburned gas that is driven by several small recirculation eddies. The flow velocity approaches stagnation conditions in the region such that stationary combustion is possible. The precise nature of the transport processes in this region is unclear and is the subject of further detailed investigation.

Figures 9 and 10 show radial profiles of density and temperature, and profiles of H_2, O_2, OH and H_2O mass fractions, respectively, at axial locations of 0.1 and 1 dimensionless units downstream of the injector tip. These plots correspond directly to the contour plots given in Figs. 6 and 7 and show the distinct nature of the shearlayer region. Though continuous, gradients in the flame zone approach the behavior of a contact discontinuity. The three order of magnitude change in density over the extremely small spatial interval is clearly evident, as is the distinct change in temperature due to combustion and scalar mixing processes. The depletion of all of the oxygen in the flame, the flame structure, and the fuel rich characteristics on the hydrogen side of the flame are also apparent. The existence of the contact discontinuity and severity of the gradients has profound implications on the modeling approach and the appropriateness of a discrete continuum treatment across the interface.

Figure 11 provides a further characterization of the shearlayer region. Here radial profiles of the compressiblity factor Z and the derivative relations,

$$\mathcal{Z}_p = \left[1 - \frac{p}{Z}\left(\frac{\partial Z}{\partial p}\right)_T\right] \tag{1}$$

$$\mathcal{Z}_T = \left[1 + \frac{T}{Z}\left(\frac{\partial Z}{\partial T}\right)_p\right], \tag{2}$$

are given at the same axial locations as Figs. 9 and 10. The compressiblity factor indicates the degree to which the local mixture state approaches that of an ideal gas. Similarly, Eqs. (1) and (2) are related to the isothermal compressibility and the coefficient of thermal expansion and indicate the degree to which these fundamental forms of compressibility deviate from that of an ideal gas. The isothermal compressibility characterizes the change in volume that results from a change in pressure while temperature remains constant. The coefficient of thermal expansion characterizes the change in volume that results from a change in temperature while the pressure remains constant. Analysis of Fig. 11 reveals that real gas effects exist locally in colder regions of the flow on either side of the shearlayer, and ideal gas characteristics exist within the hot fuel rich region and flame zone. Not surprisingly, this latter observation can be attributed to the diminished effect of pressure that occurs with increasing temperature. Fig. 11 also reveals the profound effect of the contact discontinuity on thermophysical properties. Similar studies focused on transport processes and appropriate subgrid-scale closures for high-fidelity LES simulations are currently being conducted.

CONCLUSIONS

This paper has highlighted some of the key phenomenological trends and various intricacies associated with cryogenic injection and combustion processes in liquid rocket engines. Emphasis has been placed on the first of a series of

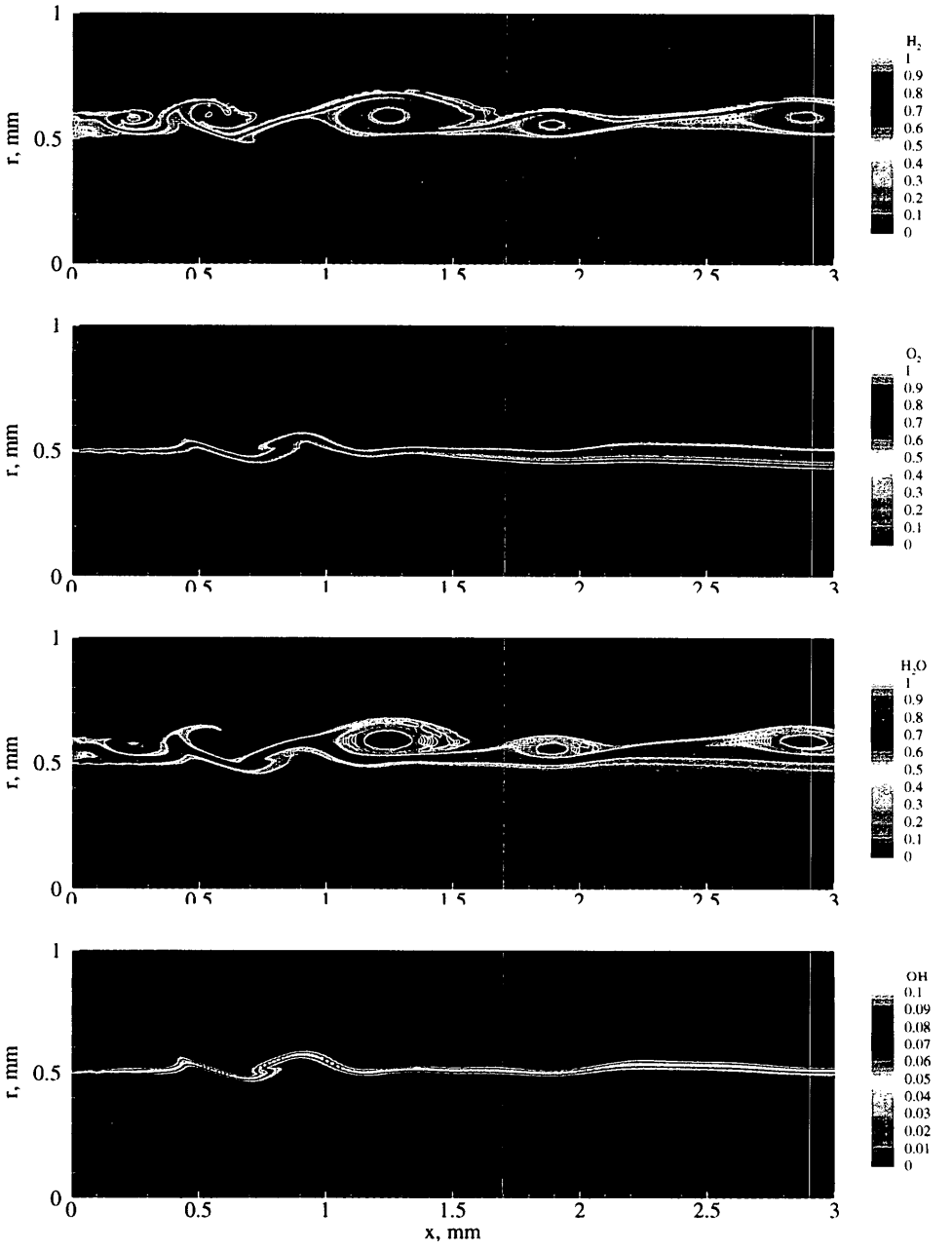

Figure 7: Contours of H_2, O_2, H_2O and OH mass fractions in the region from the injector tip to 3 diameters downstream. Chamber pressure is 10.1 *MPa* (100 atm), hydrogen (upper stream) and oxygen (lower stream) velocities are 125 and 30 m/s, respectively, and injection temperatures are 150 *K* and 100 *K*.

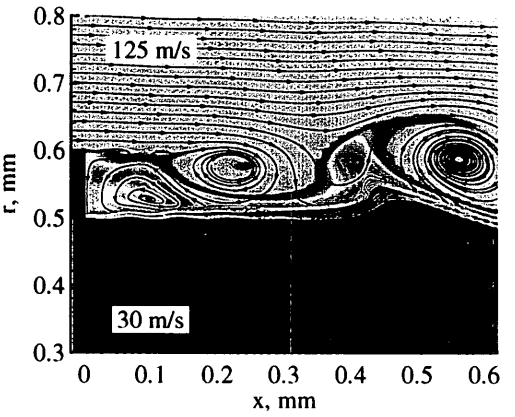

Figure 8: Streamtraces superimposed on contours of H_2 mass fraction in the vicinity of the LOX post. The legend corresponds to that given for H_2 in Fig. 7. The white contours highlight the location of the OH radicals.

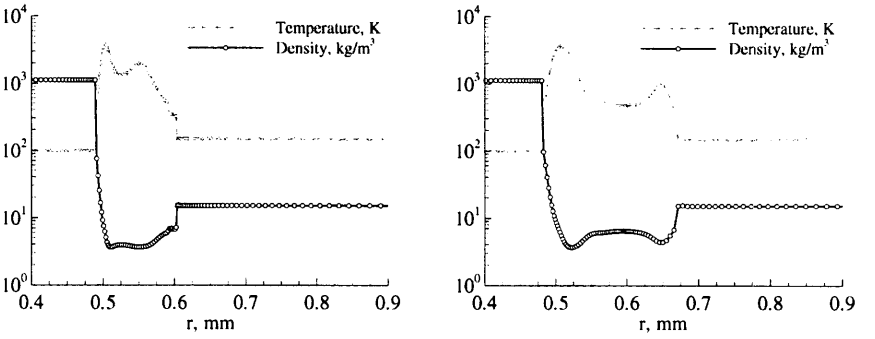

Figure 9: Radial profiles of density and temperature at axial locations of 0.1 (left) and 1 (right) dimensionless units.

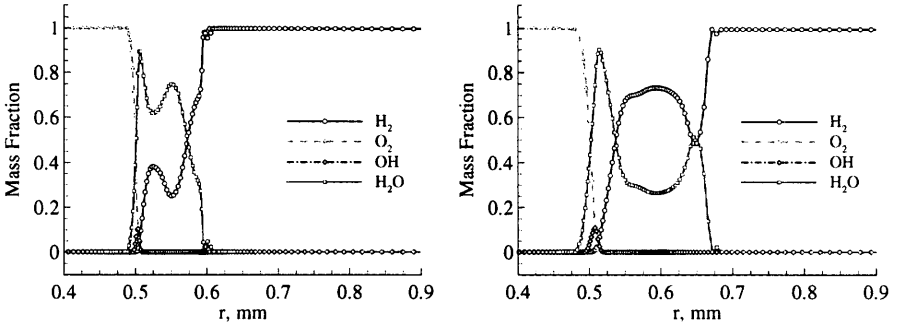

Figure 10: Radial profiles of H_2, O_2, OH and H_2O mass fractions at axial locations of 0.1 (left) and 1 (right) dimensionless units.

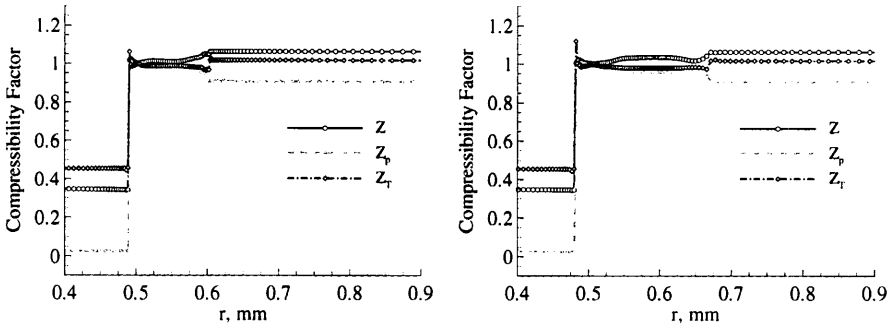

Figure 11: Radial profiles of the compressiblity factor Z and the derivative relations Z_p and Z_T at axial locations of 0.1 (left) and 1 (right) dimensionless units.

hierarchical simulations aimed at assessing the modeling requirements for application of the large eddy simulation technique. The focus was on LOX–H_2 coaxial injectors at a condition where the LOX is injected at a subcritical temperature into a supercritical environment. For this situation a diffusion dominated mode of combustion occurs in the presence of exceedingly large thermophysical property gradients. Though continuous, these gradients approach the behavior of a contact discontinuity.

The results presented have outlined some of the key phenomenological trends and have highlighted various intricacies related both to modeling and the fundamental processes involved. The existence of the contact discontinuity and severity of the gradients has profound implications on the modeling approach and the appropriateness of a discrete continuum treatment across the interface. The precise nature of the transport processes in this region is also unclear and is the subject of further detailed investigation. Both real and ideal gas behavior occurs locally in various parts of the flow. Real gas effects exist locally in colder regions of the flow. Not surprisingly ideal gas and transport characteristics occur within the fuel rich region and flame zone. The latter observation can be directly attributed to the diminished effect of pressure that occurs with increasing temperature.

Ongoing efforts will continue to focus on LES subgrid-scale model development and validation at realistic device-scale conditions. Systematic treatment of turbulent flame phenomena, for example, is still pending, as is the treatment of atomization processes. Respective analyses will also focus on injector port and duct turbulence at cryogenic conditions, further treatment and sensitivity of thermodynamic and transport properties, high-pressure thermochemistry and chemical kinetics.

ACKNOWLEDGMENTS

This work was funded by the NASA Marshall Space Flight Center under contract H-33477D. The support provided is gratefully acknowledged.

References

[1] W. Mayer and H. Tamura. Propellant injection in a liquid oxygen/gaseous hydrogen rocket engine. *Journal of Propulsion and Power*, 12(6):1137–1147, 1996.

[2] N. B. Vargaftik. *Tables on the Thermophysical Properties of Liquids and Gases*. John Wiley and Sons, Incorporated, New York, New York, 2nd edition, 1975.

[3] O. J. Haidn, editor. *Second International Workshop on Rocket Combustion Modeling*, Lampoldshausen, Germany, March 25-27 2001. The German Aerospace Center, DLR.

[4] J. C. Oefelein. General numerical framework for reacting multiphase flow with complex thermochemistry, thermodynamics and transport. Copyright 1992-2001 by J. C. Oefelein, All Rights Reserved, 2001.

[5] T. W. Leland and P. S. Chappelear. The corresponding states principle. A review of current theory and practice. *Industrial and Engineering Chemistry Fundamentals*, 60(7):15–43, 1968.

[6] J. S. Rowlinson and I. D. Watson. The prediction of the thermodynamic properties of fluids and fluid mixtures–I. The principle of corresponding states and its extensions. *Chemical Engineering Science*, 24(8):1565–1574, 1969.

[7] J. C. Oefelein. *Simulation and Analysis of Turbulent Multiphase Combustion Processes at High Pressures*. PhD thesis, The Pennsylvania State University, University Park, Pennsylvania 16802, May 1997.

[8] J. C. Oefelein and V. Yang. Modeling high-pressure mixing and combustion processes in liquid rocket engines. *Journal of Propulsion and Power*, 14(5):843–857, 1998.

[9] R. C. Reid, J. M. Prausnitz, and B. E. Polling. *The Properties of Liquids and Gases*. McGraw-Hill, New York, New York, 4th edition, 1987.

[10] G. J. VanWylen and R. E. Sonntag. *Fundamentals of Classical Thermodynamics*. John Wiley and Sons, Incorporated, New York, New York, 3rd edition, 1986.

[11] S. Gordon and B. J. McBride. Computer program for calculation of complex chemical equilibrium compositions, rocket performance, incident and reflected shocks and Chapman-Jouguet detonations. Technical Report NASA SP-273, National Aeronautics and Space Administration, 1971.

[12] R. J. Kee, F. M. Rupley, and J. A. Miller. Chemkin thermodynamic data base. Technical Report SAND87-8215B, Sandia National Laboratories, 1990. Supersedes SAND87-8215 dated April 1987.

[13] J. F. Ely and H. J. M. Hanley. Prediction of transport properties. 1. Viscosity of fluids and mixtures. *Industrial and Engineering Chemistry Fundamentals*, 20(4):323–332, 1981.

[14] J. F. Ely and H. J. M. Hanley. Prediction of transport properties. 2. Thermal conductivity of pure fluids and mixtures. *Industrial and Engineering Chemistry Fundamentals*, 22(1):90–97, 1981.

[15] R. B. Bird, W. E. Stewart, and E. N. Lightfoot. *Transport Phenomena*. John Wiley and Sons, Incorporated, New York, New York, 1960.

[16] J. O. Hirschfelder, C. F. Curtiss, and R. B. Bird. *Molecular Theory of Gases and Liquids*. John Wiley and Sons, Incorporated, New York, New York, 2nd edition, 1964.

[17] S. Takahashi. Preparation of a generalized chart for the diffusion coefficients of gases at high pressures. *Journal of Chemical Engineering of Japan*, 7(6):417–420, 1974.

[18] C. K. Westbrook and F. L. Dryer. Chemical kinetics modeling of hydrocarbon combustion. *Progress in Energy and Combustion Science*, 10(1):1–57, 1984.

[19] R. A. Yetter, F. L. Dryer, and H. Rabitz. A comprehensive reaction mechanism for carbon monoxide/hydrogen/oxygen kinetics. *Combustion Science and Technology*, 79:97–128, 1991.

[20] W. Mayer. DLR test facility P8, windowed combustor experiment BK C, In Progress. The German Aerospace Center, Lampoldshausen, Germany.

[21] W. Mayer, A. Schik, M. Schäffler, and H. Tamura. Injection and mixing processes in high-pressure liquid oxygen/gaseous hydrogen rocket combustors. *Journal of Propulsion and Power*, 16(5):823–828, 2000.